Journal of Theoretical Biology 295 (2012) 9–22

Contents lists available at SciVerse ScienceDirect

Journal of Theoretical Biology

journal homepage: www.elsevier.com/locate/yjtbi

The effects of a telomere destabilizing agent on cancer cell-cycle dynamics—Integrated modelling and experiments

Bartholomäus V. Hirt [a,*], Jonathan A.D. Wattis [a], Simon P. Preston [a], Charles A. Laughton [b]

[a] School of Mathematical Sciences, University of Nottingham, University Park, Nottingham NG7 2RD, United Kingdom
[b] School of Pharmacy, University of Nottingham, University Park, Nottingham NG7 2RD, United Kingdom

ARTICLE INFO

Article history:
Received 10 June 2011
Received in revised form
30 October 2011
Accepted 31 October 2011
Available online 18 November 2011

Keywords:
Mathematical model
Parameter estimation
Model identifiability
RHPS4
Cell death

ABSTRACT

The pentacyclic acridinium salt RHPS4 displays anti-tumour properties *in vitro* as well as *in vivo* and is potentially cell-cycle specific. We have collected experimental data and formulated a compartmental model using ordinary differential equations to investigate how the compound affects cells in each stage of the cell cycle. In addition to a control case in which no drug was used, we treated colorectal cancer cells with three different concentrations of the drug and fitted simulations from our models to experimental observations. We found that RHPS4 caused a concentration-dependent, marked cell death in treated cells, which is best modelled by allowing the rate parameters corresponding to cell death to be sigmoidal functions of time. We have shown that the model is "identifiable", meaning that, at least in principle, the parameter values can be determined from observable quantities. We find that at low concentrations RHPS4 primarily affects the cells in the G_2/M phase, and that the drug has a delayed effect with the delay decreasing at larger doses. Since the drug diffuses into the nucleus, the observed delayed effect of the compound is unexpected and is a novel finding of our research into this compound.

1. Introduction

The study of anti-cancer agents has not yet generated an efficient remedy for most of the common cancer types, which suggests that much research is still necessary to understand the processes involved in cancer development as well as the mechanisms which specific anti-cancer treatments evoke. Tissue culture experiments are frequently used to evaluate the ability of new drugs to induce growth inhibition, changes in cell-cycle progression and cell death. Comparing the results from such experiments to observations from *in vitro* experiments on cell components can bring understanding into the actual mechanisms in living cells.

The eukaryotic cell cycle consists of five major phases, namely a resting state G_0 and four cycling phases G_1, S (synthesis), G_2 and M (mitotic) phase with cells progressing in this order before dividing into two cells back in phase G_1. Growth factors activate membrane receptors of a cell triggering cell-cycle entry, and intracellular signal transduction pathways induce the activation of cyclin-dependent kinases that control the transitions between the cell-cycle phases (Aguda, 2001). Chromosome duplication, during which DNA is replicated, occurs during the S phase. Due to specific mechanisms of DNA synthesis, telomeres, the terminating DNA sequences at chromosome ends, shorten during cell division (Levy et al., 1992). When telomeres reach a certain threshold length called the Hayflick limit, cells enter a non-dividing state (senescence), where cells remain viable until they normally undergo a controlled form of cell death (apoptosis), which is often accompanied by DNA degradation at later stages. The enzyme telomerase, however, can antagonise telomere attrition by telomere elongation, and this happens in about 90% of cancerous cells (Kim et al., 1994).

The compound RHPS4 (3,11-difluoro-6,8,13-trimethyl-8*H*-quino [4, 3,2−*kl*] acridinium methosulphate) is a potential anti-cancer drug which has been found (Gavathiotis et al., 2003; Cheng et al., 2008) to interfere with DNA replication processes that are part of the cell cycle. Investigating the cell cycle dynamics can give insight into whether we find similar behaviour in living cells.

The drug RHPS4 stabilises guanine-rich structures at telomeric ends inhibiting the binding of telomerase (Gowan et al., 2001). The compound is an attractive agent because of its ability to shorten telomeres by telomerase inhibition via exposure of cells at low concentrations. Cookson et al. (2005a) showed a significant reduction in telomere length of MCF-7 breast cancer cells when treated with subtoxic doses of RHPS4. Moreover, the drug can also rapidly induce telomere dysfunction by altering telomeric chromatin leading to short-term cell death at higher doses (Salvati et al., 2007). RHPS4 reduced the growth of human tumours xenografted in mice *in vivo* and did not show any toxic effect in mice. Additionally, treatment with RHPS4 of human melanoma

* Corresponding author. Tel.: +44 7546120150.
E-mail address: pmxbvh@nottingham.ac.uk (B.V. Hirt).

0022-5193/$ - see front matter © 2011 Elsevier Ltd. All rights reserved.
doi:10.1016/j.jtbi.2011.10.038

lines, possessing relatively long telomeres, resulted in a dose-dependent decrease in cell replication and accumulation of cells in the S-G_2/M phase of the cell cycle after 6 days (Leonetti et al., 2004).

Mathematical modelling can be a useful means for integrating different types of experimental data in medical applications to predict the mechanism of action of compounds to be investigated (Wolkenhauer et al., 2009). Modern experimental techniques generate a vast amount of data that have to be interpreted and systematic information be extracted, which is often beyond the scope of traditional techniques. For instance, the development of mathematical models is essential to deal with the complexity of cell cycle processes and cell cycle regulation (Fuss et al., 2005), which are an important part of cancer development studies in biotechnology and medicine.

A variety of mathematical models of the cell cycle can be found in the literature. A quantitative description of cell cycle dynamics based on the time cells spend in each phase of the cell cycle is presented by Montalenti et al. (1998). Panetta and Adam (1995) developed a two-compartment ordinary differential equation (ODE) model of cycling and resting cells. Sherer et al. (2008) used a partial differential equation (PDE) model consisting of three compartments which represent the G_0+G_1 phase, the S phase and the G_2+M phase. DNA histograms of the total cell population provide data for this model, which can be used to estimate corresponding transition rate functions. More detailed models, distinguishing further between single phases of the cell cycle, use mixtures of ODEs and PDEs, as proposed by Basse et al. (2005), Basse and Ubezio (2007) and Venkatasubramanian et al. (2008). In addition, several models of cell cycle regulation describing molecular interactions in different pathways of the cell cycle control apparatus are given by Tyson (1991), Tyson and Novak (2001) and Yang et al. (2006). Further references regarding cell cycle models of tumour development and spatio-temporal response to cell-cycle specific anti-cancer agents can be found in Johnson et al. (2011).

We use a systems biology approach to investigate how the drug RHPS4 changes the cell cycle dynamics over short periods of time and at medium drug concentrations (50–1000 nM). We formulate a novel cell-cycle model distinguishing between viable and dead cells of the same DNA content and report results of the best fit of model to experimental data. Our method involves new experimental design, the application of effective parameter estimation, and statistical model evaluation techniques to gain a more detailed insight into the actual dynamics of cells in drug assays and more information on the accuracy of the results obtained.

To keep the model structure simple we develop an ODE model based on the experimental data, where we assume that the phase of resting cells is negligible, as cells from the HCT116 cell line in our experiments have a relatively high doubling rate. We also simplify our model by including senescent cells into the compartment of G_0/G_1 cells, as the proportion of senescent cells in an RHPS4 assay does not substantially change over the time-scale of 10 days (Johnson et al., 2011), which we use in our assays. Our model allows for cell death from all cell-cycle phases and we distinguish between early and late stages of cell death, the latter of which being characterised by DNA fragmentation processes.

In Section 2 we present the mathematical model of cell-cycle dynamics and introduce a statistical model which we use to describe the experimental data. Numerical methods involved in the estimation of cell cycle parameters and statistical techniques for model inference and comparison are given in Section 3 followed by a summary of the experimental results and the results from model fitting in Section 4. Information given in Section 4 includes an analysis of the accuracy of model-data fit and an investigation of the biological implications of our results. Discussion of the presented work and conclusions are drawn in Section 5.

2. Mathematical model formulation

2.1. Model of cell cycle dynamics

The aim of our model is to find how the drug RHPS4 affects cells of the HCT116 line through their cell cycle and growth. In order to compare simulations from mathematical models to real dynamics, we have used a flow cytometer to measure the DNA content of cells and derived cell cycle distributions by evaluating the corresponding DNA histograms. Viable cells were distinguished from dead cells by trypan blue dye exclusion, and the total number of cells in each cell population was determined daily for 10 days. Our model is constructed according to experimental data collected in the tissue culture laboratory (see Appendix A for the experimental techniques).

The proportions of viable and dead cells and proportions of cells in the phases, G_0/G_1, S, G_2/M, of the cell cycle have been collected under control conditions and under treatment with different concentrations (50 nM, 100 nM and 1 μM) of the potential anticancer drug RHPS4 over 10 days. The phases G_0/G_1, S, G_2/M have been distinguished by their DNA content in a cell, being onefold during the phases G_0 and G_1, twofold during phases G_2 and M, and between one- and twofold during the synthesis phase S. Cells identified to be in one of these cell cycle phases are either viable or have been measured a short time after the onset of cell death. Pre-G_1 cells are dead cells being detected some time after the onset of cell death and contain fragmented DNA with less DNA content than a G_0/G_1 cell. A cell cycle model of viable cells is depicted in Fig. 1. Cell death is indicated by loss of cell material from each of the three cell-cycle phases.

The cell states that can be detected suggests the assignment of seven compartments, namely X, Y, Z for viable cells being in G_0/G_1, S, G_2/M, respectively, $\overline{X}$, $\overline{Y}$, $\overline{Z}$ for cells dying recently in each of the cell-cycle phases, and A for all pre-G_1 cells. However, experimental measurements do not allow us to distinguish between viable and dead cells of the same DNA content. The observable states therefore differ from the classification, we can only observe cells in $X+\overline{X}$, $Y+\overline{Y}$, $Z+\overline{Z}$, $X+Y+Z$, $\overline{X}+\overline{Y}+\overline{Z}+A$ and A.

Viable cells go around the cell cycle $X\to Y\to Z\to 2X\to\ldots$, where cells double in number at the transfer from Z to X. It is possible that cells die from each of the phases G_0/G_1, S, G_2/M of the cell cycle, that is, $X\to\overline{X}$, $Y\to\overline{Y}$ and $Z\to\overline{Z}$. Once cells have died, their DNA cannot be synthesised anymore and their nucleus is subject to DNA degradation, hence $\overline{X}\to A$, $\overline{Y}\to A$, $\overline{Z}\to A$. Fig. 2 illustrates the 7-compartment model including the observable states.

We use the principle of mass action to model the dynamics with the following system of ODEs

$$\frac{dX}{dt}=2k_{ZX}Z-(k_{XY}+k_{X\overline{X}})X, \tag{1}$$

$$\frac{dY}{dt}=k_{XY}X-(k_{YZ}+k_{Y\overline{Y}})Y, \tag{2}$$

$$\frac{dZ}{dt}=k_{YZ}Y-(k_{ZX}+k_{Z\overline{Z}})Z, \tag{3}$$

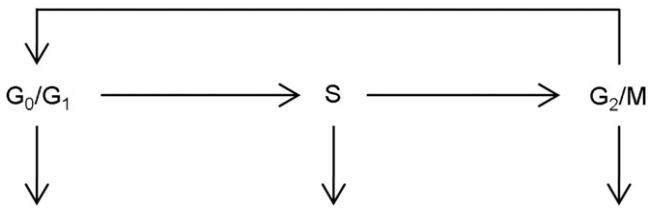

Fig. 1. A cell cycle model of viable cells including death from each of the three phases.

$$\frac{d\overline{X}}{dt} = k_{X\overline{X}}X - k_{XA}\overline{X}, \tag{4}$$

$$\frac{d\overline{Y}}{dt} = k_{Y\overline{Y}}Y - k_{YA}\overline{Y}, \tag{5}$$

$$\frac{d\overline{Z}}{dt} = k_{Z\overline{Z}}Z - k_{ZA}\overline{Z}, \tag{6}$$

$$\frac{dA}{dt} = k_{XA}\overline{X} + k_{YA}\overline{Y} + k_{ZA}\overline{Z}, \tag{7}$$

with initial values $(X,Y,Z,\overline{X},\overline{Y},\overline{Z},A)^T|_{t=0} = (X_0,Y_0,Z_0,\overline{X}_0,\overline{Y}_0,\overline{Z}_0, A_0)^T \geq \mathbf{0}$ being non-negative. Transition rates between compartments are denoted by k subscripted with labels corresponding to relevant compartments (e.g. k_{XY} is the rate of transition from the X to the Y compartment) and are assumed to be non-negative and constant. The nature of the experimental data presented later (in Section 4) suggests that we allow the rate coefficients governing transition from viable cells to dead cells to be time-dependent, that is we let $k_* = k_*(t)$ where $(*)$ represents $X\overline{X}$, $Y\overline{Y}$, or $Z\overline{Z}$.

We have used several models for the transition rate functions $k_*(t)$ to fit the 7-compartment model to experimental data, a choice of which is given in Fig. 3. The basic rate functions describe

(M_0) constant behaviour: $k_*(t) = k_{*0}$,

(M_1) a sigmoidal increase: $k_*(t) = k_{*0} + \Delta k_* - \Delta k_*/(1+(t/t_0)^{\beta})$,

the change occurring around the time point t_0, where the magnitude of the increase in rate $k_*(t)$ is Δk_* and β is a shape parameter. Note that the rate function model M_0 is the special case of M_1 with $\Delta k_* = 0$. The choice of each of the parameters in the transition functions will later be evaluated and the best model chosen to find the most appropriate description of the cell cycle dynamics for each drug concentration.

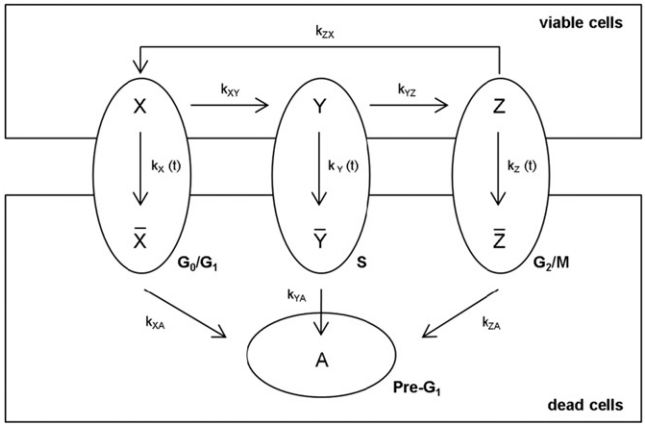

Fig. 2. A 7-compartment model with compartments X, Y, Z, $\overline{X}$, $\overline{Y}$ $\overline{Z}$, A, arising from the nature of the collected data in Appendix A. Transition rates k_* between compartments are assumed to be constant except for k_X, k_Y, k_Z possibly being time-dependent functions. We group together the observed quantities, that is the number of cells in each phase G_0/G_1, S, G_2/M, pre-G_1 (oval), and viable, dead cells (rectangular areas).

2.2. Statistical model of experimental data

It is helpful to write the model (1)–(7) in vector form: The cell-cycle dynamics are modelled by a system of ODEs of the form

$$\frac{d\mathbf{v}(t,\mathbf{p})}{dt} = \mathbf{A}(t,\boldsymbol{\theta})\mathbf{v}(t,\mathbf{p}), \quad 0 \leq t \leq t_e, \tag{8}$$

$$\mathbf{v}(0,\mathbf{p}) = \mathbf{v}_0, \tag{9}$$

where $\mathbf{v}$ is the m-dimensional vector of state variables and t denotes the time in the interval $[0,t_e]$. The parameter vector $\mathbf{p} = (\boldsymbol{\theta},\mathbf{v}_0)$ with domain $\boldsymbol{\Theta} \subseteq \mathbb{R}^L$ is an L-dimensional vector of l unknown rate parameters $\boldsymbol{\theta}_k$, $k = 1,\ldots,l$, and m initial conditions $(\mathbf{v}_0)_j$, $j = 1,\ldots,m$, $(L = l+m)$ and $\mathbf{A}$ is an $m \times m$ matrix with entries that depend on $\boldsymbol{\theta}$ and possibly t. For example, for rate model M1, we have $t_e = 10$, $m = 7$, $l = 13$, $L = 20$, $\mathbf{v} = (X,Y,Z,\overline{X},\overline{Y},\overline{Z},A)^T$ and

$$\boldsymbol{\theta} = (k_{XY},k_{YZ},k_{ZX},k_{X\overline{X}0},\Delta k_{X\overline{X}},k_{Y\overline{Y}0},\Delta k_{Y\overline{Y}},k_{Z\overline{Z}0},\Delta k_{Z\overline{Z}},t_0,k_{XA},k_{YA},k_{ZA}). \tag{10}$$

Whilst our model has $m = 7$ quantities $(X,Y,Z,\overline{X},\overline{Y},\overline{Z},A)$, only $M = 5$ independent quantities are measured, respectively $w_1 = X+\overline{X}$, $w_2 = Y+\overline{Y}$, $w_3 = Z+\overline{Z}$, $w_4 = X+Y+Z$ and $w_5 = A$. Hence the vector $\mathbf{w}$ of measurements obtained is a linear combination of $\mathbf{v}$, this is, $\mathbf{w} = \mathbf{B}\mathbf{v}$, where

$$\mathbf{B} = \begin{pmatrix} 1 & 0 & 0 & 1 & 0 & 0 & 0 \\ 0 & 1 & 0 & 0 & 1 & 0 & 0 \\ 0 & 0 & 1 & 0 & 0 & 1 & 0 \\ 1 & 1 & 1 & 0 & 0 & 0 & 0 \\ 0 & 0 & 0 & 0 & 0 & 0 & 1 \end{pmatrix}. \tag{11}$$

Before estimating parameters it is useful first to check whether the model (1)–(7) is identifiable (see Walter and Pronzato, 1996 for a review of identifiability analysis). An identifiable model is one for which the unknown parameters of the model, our rates k_*, can be uniquely recovered from the observed data under ideal conditions, that is, assuming we have error-free and continuous data for all observables available. We have confirmed using the transfer function method (Cobelli and Distefano, 1980; Jacquez, 1996) that our model is identifiable.

In our model the observables w_j are observed with noise. Hence we model w_j as a random variable W_j. Our statistical model for $W_j(t_i)$, $j = 1,\ldots,M$, $i = 1,\ldots,n$, the jth observable at ith time point, is

$$\ln W_j(t_i) = \ln(\mathbf{B}\,\mathbf{v}(t_i,\mathbf{p}))_j + \boldsymbol{\varepsilon}_{ij}, \tag{12}$$

where $\boldsymbol{\varepsilon}_{ij}$ are the measurement errors, which we assume are independently and identically distributed as $\boldsymbol{\varepsilon}_{ij} \sim N(0,\sigma^2)$ with variance σ^2. This choice of error distribution seems appropriate

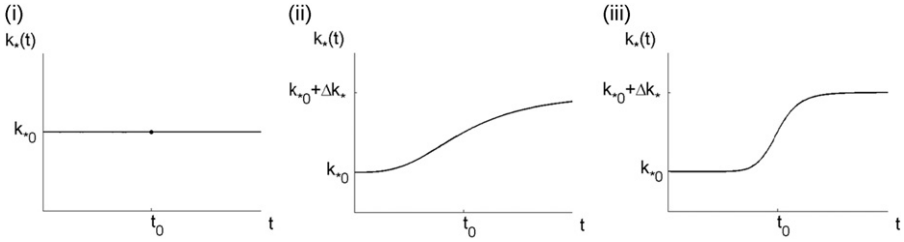

Fig. 3. A schematic illustration of (i) rate model M_0 and rate model M_1 with (ii) small β and (iii) large β, governing transition from viable cells to dead cells in the 7-compartment model in Fig. 2. k_{*0} denotes the initial rate of cell death, t_0 the time point of the onset of significant cell death, Δk_* the magnitude of the increase in rate and n is a shape parameter of model M_1.

since the data stem from an autocatalytic growth process, that is a replication process, in which Gaussian variation in the growth rates will generate a log-normal error structure in the obtained cell numbers (Koch, 1966; Limpert et al., 2001).

3. Numerical methods/analysis

3.1. Parameter estimation

The parameters to be estimated in our model (12) are a maximum of $l=13$ rate parameters $\boldsymbol{\theta}_k$ and $m=7$ initial conditions $(\boldsymbol{v}_0)_j$ whose values are not known exactly. We use a least squares approach for determining optimal parameter values. The approach is equivalent to maximising the likelihood function under model (12), that is, maximising the probability that, for a given parameter vector $\boldsymbol{\alpha}=(\mathbf{p},\sigma)$, certain realisations $w_i(t_i)$ of the random variables $W_j(t_i)$ occur, interpreted as a function of $\boldsymbol{\alpha}$. The sum of the squared residuals is

$$f(\mathbf{p})=\sum_{i=1}^{n}\sum_{j=1}^{M}\mathbf{e}_{i,j}^2(\mathbf{p}), \tag{13}$$

where

$$\mathbf{e}_{i,j}(\mathbf{p})=\ln(\mathbf{Bv}(t_i,\mathbf{p}))_j-\ln w_j(t_i). \tag{14}$$

The least-squares parameter estimate is

$$\hat{\mathbf{p}}=\arg\min_{\mathbf{p}\in\boldsymbol{\Theta}} f(\mathbf{p}), \tag{15}$$

which we compute using a Stochastic Ranking Evolutionary Strategy (SRES) (Runarsson and Yao, 2000) followed by local optimisation using the Levenberg–Marquardt (LM) method. SRES uses the idea of treating parameter sets as the 'genome' of an individual and a procedure of selection, recombination and mutation is repeated over G generations to find an optimal parameter set. We performed calculations in MATLAB using an ODE solver (ode45) for the numerical integration of (1)–(7), using the implementation from Kleinstein et al. (2006) with $G=500$ for the SRES algorithm, and using the function lsqnonlin for the LM optimisation.

3.2. Practical identifiability: accuracy of parameter estimates

Besides calculating $\hat{\mathbf{p}}$, we can also characterise the accuracy of this estimate. By an asymptotic result (Seber and Wild, 1989), the approximate sampling distribution of $\hat{\mathbf{p}}$ under the model assuming the true parameter value $\mathbf{p}^*$, is

$$\hat{\mathbf{p}}\sim\mathcal{N}_L(\mathbf{p}^*,\hat{\boldsymbol{\Sigma}}), \tag{16}$$

where $\mathcal{N}_L(\cdot,\cdot)$ denotes the L-dimensional multivariate normal distribution and $\hat{\boldsymbol{\Sigma}}=\mathbf{Cov}(\hat{\mathbf{p}})$ denotes the covariance matrix of the least-squares parameter estimate. The covariance matrix of $\hat{\mathbf{p}}$ indicates whether parameters are practically identifiable, that is, whether we can accurately infer values for the parameters. If we assume that the model residuals $\mathbf{e}_{i,j}(\mathbf{p})$ are approximately linear in a small neighbourhood of $\hat{\mathbf{p}}$, we can derive the covariance matrix of $\hat{\mathbf{p}}$ from linear regression analysis (Ashyraliyev et al., 2008), that is

$$\hat{\boldsymbol{\Sigma}}=\hat{\sigma}^2(\mathbf{J}_{\mathbf{F}}(\hat{\mathbf{p}})^T\mathbf{J}_{\mathbf{F}}(\hat{\mathbf{p}}))^{-1}, \tag{17}$$

where $\mathbf{F}$ is a vector function in $\mathbf{p}$ obtained by stacking the columns $\mathbf{e}_{*,j}$, $j=1,\ldots,M$, of the matrix $(\mathbf{e}_{i,j})$ into a vector, and

$$\mathbf{J}_{\mathbf{F}}(\mathbf{p})=\left(\frac{\partial\mathbf{F}_i(\mathbf{p})}{\partial\mathbf{p}_k}\right), \tag{18}$$

is the Jacobian of $\mathbf{F}$ of size $N\times L$. The quantity $\hat{\sigma}^2=f(\hat{\mathbf{p}})/(N-L)$ is an unbiased estimator of σ^2, where $N=M\times n$ is the number of experimental measurements. The diagonal elements of $\hat{\boldsymbol{\Sigma}}$ are the marginal variances of the parameter estimates $\hat{\mathbf{p}}_k$, $k=1,\ldots,L$.

3.3. Model selection

Having found best fits for both models M_0 and M_1 to experimental data, the most appropriate model for each of the given drug concentrations has to be selected. A danger in choosing a model which is meant to describe the observations from certain experiments, is overfitting the experimental data by introducing many parameters. We prefer to choose the model with the smallest number of parameters, which still describes the underlying dynamics sufficiently well. The Akaike information criterion (Akaike, 1974) (AIC) is an information-theoretic criterion for model comparison, which incorporates not only the objective function value $f(\hat{\mathbf{p}})$ but also a penalty based on the number of parameters in the model, hence it characterises the trade-off between goodness of fit and model complexity. When comparing two models according to the Akaike criterion, they must be 'nested' in the sense that the parameter space of one model is a lower dimensional subspace of the other model. The value of the Akaike criterion is given by

$$\mu_{\mathrm{AIC}}=N\ln(f(\hat{\mathbf{p}}))+2(L+1), \tag{19}$$

where N is the number of experimental measurements, f is the sum of the squared residuals and L is the number of parameters which have been fitted to the data (L is the sum of the number of rate parameters (l) and the number of initial conditions (m)) in each model. The correction term

$$\mu_{c\mathrm{AIC}}=\mu_{\mathrm{AIC}}+\frac{2(L+1)(L+2)}{N-L-2}, \tag{20}$$

(Bedrick and Tsai, 1994) should be used for smaller sample sizes, $N\leq 40(L+1)$. The candidate model with the *smallest* value μ_{AIC} is the selected model.

4. Results

4.1. Experimental results

We have measured cell cycle distribution and cell growth experimentally and have produced normalised data sets as described in Appendix A. Day 1 is the first day of analysis when measurements have been taken. We observe that control cells grow exponentially between day 1 and day 9 as represented by the approximately linear increase for $\log N(t_i)$, $i=1,\ldots,10$, the logarithm of the total cell number, plotted in Fig. 4. The data point of control cells at t_{10} is markedly lower than the data point at t_9, which is due to confluence and probably nutrient deficiency in the wells; we therefore disregard this data point in our analysis. Error bars result from the standard deviation over six replicates and are rather small (around 10%). It is important to note that they do not account for variability within different cell batches or repeated experiments incorporating intermediate breaks, as the replicates were obtained from cells of the same batch being seeded in six parallel wells. Further comments on the particular cell behaviour can be found in the discussion section.

For treated cells, we observe growth inhibition, and in general cell growth declines with increasing drug concentration. The total number of doublings at day 4 is 3.78 for control cells, 3.18 for 50 nM, 2.15 for 100 nM and 1.56 for 1 μM. A considerable growth reduction occurs after a period of 6–7 days for 50 nM, 3–5 days for 100 nM and 3–4 days for 1 μM of RHPS4, and respective total cell numbers begin to level off thereafter.

The average proportion of dead cells was around 14% for control cells, and low proportions of pre-G_1 cells (cells with

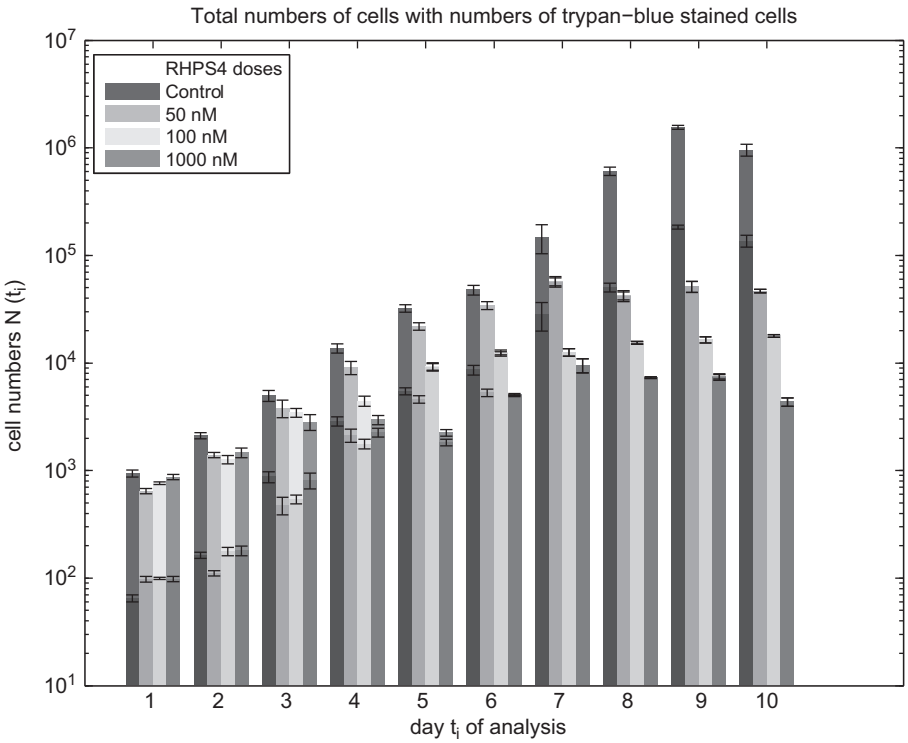

Fig. 4. Total numbers $N(t_i)$ of cells and the numbers of dead cells (measured by trypan blue dye-exclusion, lower proportion of each bar) for no drug and each drug concentration (50 nM, 100 nM, 1 μM) of RHPS4 are shown on a log scale at day t_i, $i=1,\ldots,10$ of analysis. Error bars represent the standard deviations of the corresponding values.

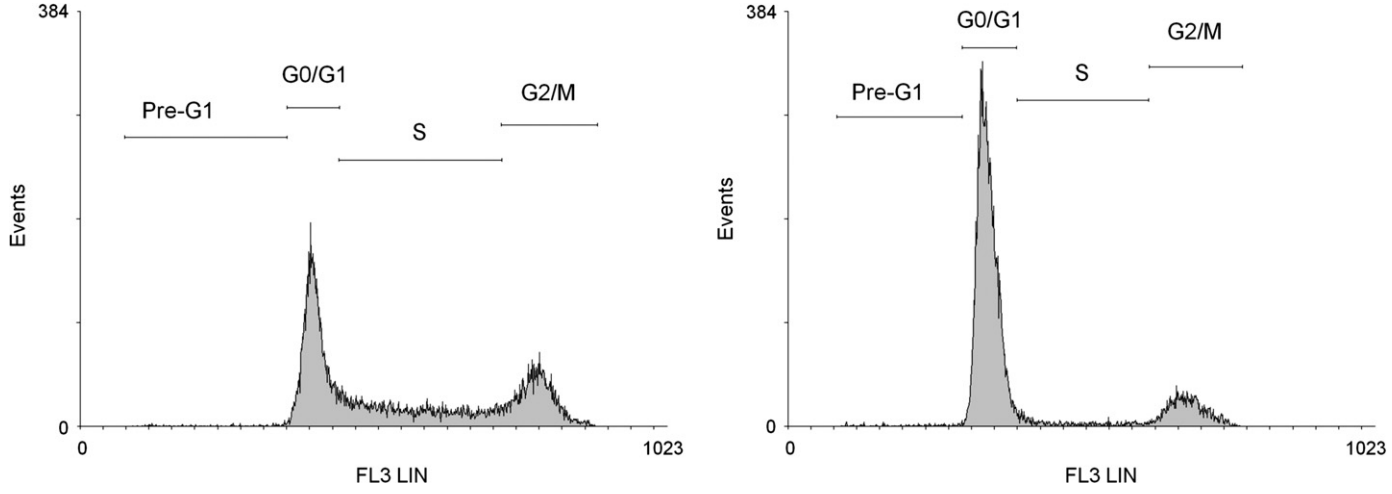

Fig. 5. Distributions of the DNA content for control cells analysed at day 4 (left) and day 10 (right) with manually set gates for the estimation of the corresponding cell cycle distributions.

fragmented DNA) at less than 5% were observed. Without treatment, the proportion of S phase and G_2/M phase cells ranged from 4% to 28% and from 8% to 30%, respectively, over the period of observation. These proportions tended to decrease gradually from higher to lower levels. Accordingly, the proportions of G_0/G_1 cells increased from 50% to 80%, that is, control cells progressively accumulated in the G_0/G_1 phase.

Interestingly, the proportion of treated cells in the S phase tended to drop from around 25% at the beginning of the experiment to about 8.5% on average by day 4 and returned to a slightly higher level of around 15% after this drop. The most dramatic effect was achieved with 1 μM of drug when the S phase proportions dropped to about 5% at day 4. The proportions of G_2/M cells behaved in a similar way but with less remarkable trends, 30% at day 1 decreasing to 20% at day 4 and 18% on average during the subsequent days. The proportion of cells in the G_0/G_1 phase increased during the first 4 days from an average of 45%–65% and thereafter decreased to around 50% for all treated cells. Before the onset of considerable cell death, the proportions of pre-G_1 cells remained at a low level of about 1–4% for all drug concentrations, and then increased to around 25%, where the increase occurred at a later time point, day 9, for the highest drug concentration. Strikingly, in the experiments with 50 nM and 100 nM of RHPS4, the proportions of pre-G_1 cells were observed to go down again after day 7, to around 3–14%, which is possibly due to disintegration of dead cells in media. Typical DNA distributions were obtained from the flow cytometer at days 4 and 10 and are shown for control cells in Fig. 5 and for cells treated with 1 μM RHPS4 in Fig. 6.

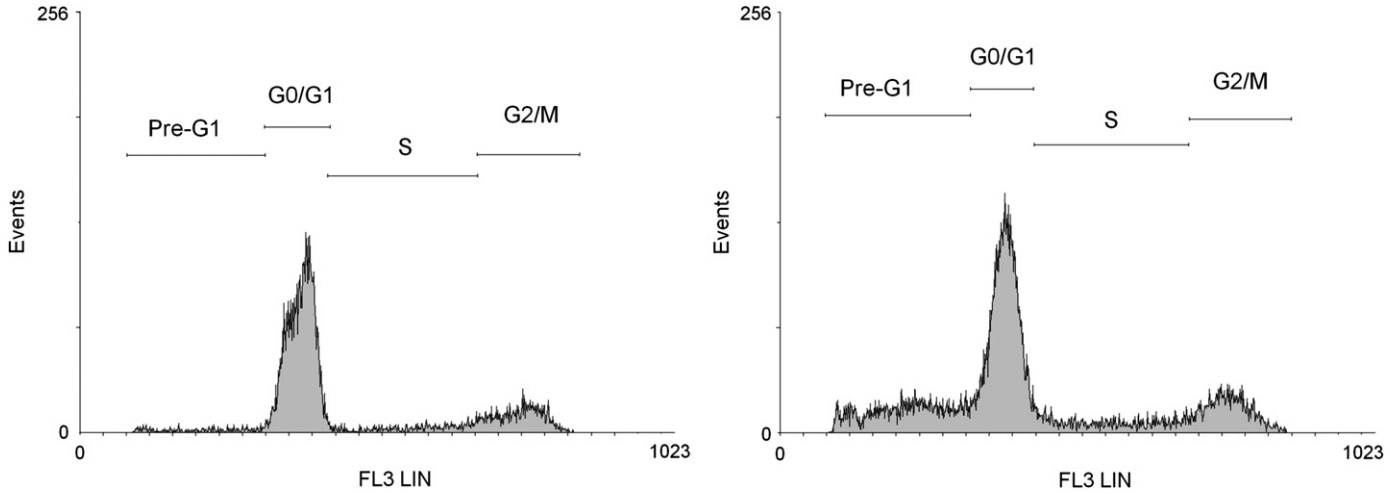

Fig. 6. Distributions of the DNA content for cells treated with 1 μM of RHPS4 analysed at day 4 (left) and day 10 (right) with manually set gates for the estimation of the corresponding cell cycle distributions.

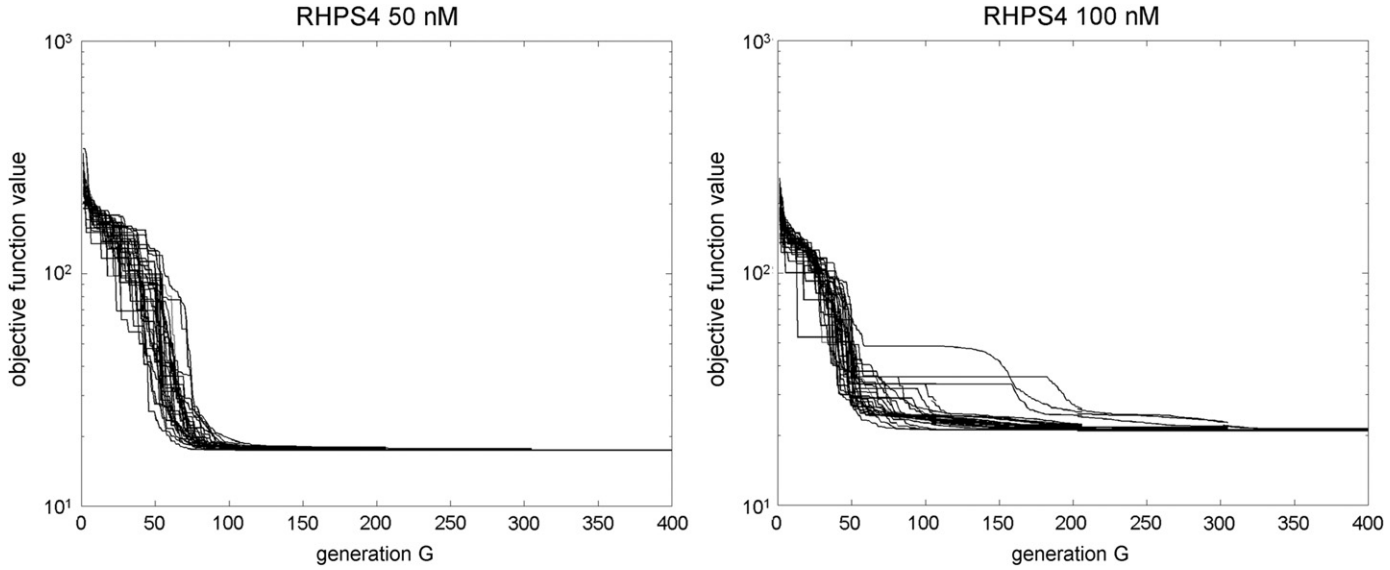

Fig. 7. The objective function values $f(\mathbf{p})$ are plotted against generation number G for several repeats of the optimisation routine with a logarithmic scale for the ordinate. The results of fitting model M_1 to data from HCT116 cells treated with 50 nM and 100 nM of RHPS4 are shown. The algorithm converges especially rapidly during the first 100 generations, and 30 repeats have been run over 500 generations to identify the global minimum.

Marked cell death (trypan blue staining) was observed at day 7 for 50 nM, at day 5 for 100 nM and at day 4 for 1 μM of RHPS4, when nearly all cells died abruptly from a prior level of around 15% at the beginning of the experiment. The intensive cell death set in more abruptly for lower drug concentrations than for higher doses. Altogether, the drug RHPS4 seems not only to affect entry into the cell cycle ($S/G_2/M$ phases) around day 4, but also to inhibit cell growth up to a complete cessation of the replication processes with increasing drug concentration.

4.2. Results of best fit of mathematical model

We fitted the submodels M_0 and M_1 (see Fig. 3) to the experimental data from each of the different treatments with RHPS4 to investigate the cell cycle dynamics described by the transition rates k of cells moving between cell-cycle phases. Estimating the initial conditions directly from experimental data did not notably influence the best fit and resulted in a higher accuracy for the estimated rate parameters (more than 75% reduction in standard errors). We chose estimates of initial values $\mathbf{v}_0$ according to experimental data at day 1 assuming that cells do not replicate during the first day of incubation and that the proportions of viable cells in each of the cell-cycle phases G_0/G_1, S, G_2/M do not differ from the proportion of viable cells across the total cell population at day 1.

We used the global optimisation method to find that the parameter estimate $\hat{\mathbf{p}}$ converged rapidly to close proximity of the global minimum during the first $G=100$ generations (see Fig. 7), and in every case of the 30 repeated runs of the SRES algorithm, based each time on a different random initial guess for $\hat{\mathbf{p}}$, the final cost function values were found to be close to the minimal cost. The parameter values obtained from the repeated runs of the SRES+LM routine showed (see Supplementary Material for an illustration of the case of 50 nM RHPS4) that the convergence of the method is relatively stable and a unique minimum could be identified.

We calculated μ_{cAIC} to select between M_0 and M_1, for each drug concentration. Table 1 shows the values of μ_{cAIC}, as well as the values of the cost function f and the variance estimates $\hat{\sigma}^2$, suggesting that model M_0 describes best the behaviour of control

cells and model M_1 the dynamical behaviour of treated cells. A value of $\beta=10$ was used for model M_1 (sigmoidal rate increase) as smaller values of β resulted in worse fits. In particular, values of $\beta \leq 3$ did not fit the data showing that the drug introduces not gradual but abrupt changes in the number of viable cells. Note that, for control cells, the model with a higher cost function value but a smaller number of parameters has been chosen. For increasing drug concentration, the data variance estimator increases from about 0.2 (control) to 0.5 (1 μM RHPS4) indicating that more variability occurs in the data at higher doses of RHPS4.

We found very low parameter values for $k_{Y\bar{Y}0}$ and $k_{Z\bar{Z}0}$ in control cells, which causes parameter identifiability problems for k_{YA} and k_{ZA}, as the choice of those parameter values, with $\bar{Y}$, $\bar{Z}$ being practically zero, did not influence the model dynamics significantly. Therefore, we refitted model M_0 with only five parameters, setting $k_{Y\bar{Y}0}=k_{Z\bar{Z}0}=k_{YA}=k_{ZA}=0$. The choice of the reduced model, denoted by M_0^*, resulted in similar parameter fits (see Table 2), but a smaller value of μ_{cAIC} (Table 1) compared to model M_0, confirming the model reduction.

Similarly, we reduced model M_1 by setting $k_{Y\bar{Y}0}=k_{Z\bar{Z}0}=k_{YA}=k_{ZA}=0$ for cells treated with higher drug concentrations (model M_1^*) and setting $k_{X\bar{X}0}=k_{Y\bar{Y}0}=k_{XA}=k_{YA}=0$ for treatment with 50 nM RHPS4 (model M_1^{**}). This has been suggested by all of those parameters k_{*0} satisfying $k<10^{-6}$/day, with parameters k_{*0} that have not been removed taking values larger than 10^{-1}/day. Furthermore, lower μ_{cAIC} values for model M_1^* and model M_1^{**} than for model M_1 supported our choice of model reduction.

There is good agreement between model predictions of the selected models and experimental data, especially for control and 50 nM of RHPS4. The simulated and observed data are shown for each concentration and each observed quantity in Fig. 8. For higher drug concentrations, the simulations overestimate the number of S phase cells at day 4. However, there is more noise in the data with increasing concentration of RHPS4, and the model still captures the major trend of the cell cycle dynamics well.

4.3. Parameter fitting—model results

The simulations of the dynamical behaviour of viable cells confirm that control cells grow exponentially, with the number of G_0/G_1 cells being larger than the number of G_2/M cells and the G_2/M cell numbers being slightly larger than the number of S-phase cells across the observation period. The doubling time $T_d=19.8$ h simulated for control cells is within biological variability of the value $T_d=20.5$ h quoted by Brattain et al. (1981). Cells die from the G_0/G_1 phase, the number of non-viable S-phase and G_2/M-phase cells remain at a constant, very low level (see left panel of Fig. 9). Note that t has been shifted one unit to the left in the diagrams in accordance with the first measurements being on day 1 of the experiments, so this is when we assume cell growth to start.

When the drug is added to the cells, the cell cycle dynamics change markedly. The numbers of viable cells in each phase of the cell cycle decay exponentially after an initially exponential increase and nearly vanish at the end of the observation period (see right panel of Fig. 9 for 50 nM and Fig. 10 for 100 nM and 1 μM RHPS4). Whereas the rate ξ_s of the exponential increase does not differ much across treatments ($\xi_s \in [0.6/\mathrm{day}, 0.8/\mathrm{day}]$, setting $k_*(t)=k_{*0}$ in Appendix B), exponential decrease occurs with rates ($\xi_s=-2.2458$/day for 50 nM, $\xi_s=-0.98828$/day for

Table 1
The optimal objective function values $f_{\min}=f(\hat{\mathbf{p}})$ and variance estimates $\hat{\sigma}^2$ for the model residuals are given for models M_0 and M_1 and each concentration of the drug RHPS4, and the model fits are compared with respect to their values μ_{cAIC} of the corrected Akaike criterion. Data of model M_0^* is given for 0 nM, of model M_1^* for 100 nM and 1 μM, and of model M_1^{**} for 50 nM RHPS4 only. The 'best' model is chosen according to the lowest value of μ_{cAIC}.

RHPS4	Model type	$f_{\min}$	$\hat{\sigma}^2$	μ_{cAIC}	Model chosen
0 nM	M_0	8.1856	0.189	138.64	
	M_1	7.9739	0.194	150.88	
	M_0^*	8.2152	0.168	127.51	✓
50 nM	M_0	118.29	2.319	310.88	
	M_1	17.481	0.372	209.00	
	M_1^{**}	17.481	0.343	196.16	✓
100 nM	M_0	50.604	0.992	259.93	
	M_1	20.985	0.446	219.96	
	M_1^*	20.985	0.411	207.12	✓
1 μM	M_0	36.423	0.714	240.20	
	M_1	26.038	0.554	232.91	
	M_1^*	26.038	0.511	220.06	✓

Table 2
Results of parameter estimation. The transition rates k are displayed in units of 1/day for all concentrations of the drug RHPS4, together with respective residence times T_X, T_Y, T_Z of cells in the G_0/G_1, S, G_2/M phase and doubling times T_d of viable cells (before the time of marked cell death) given in units of hours. Cells die with rates $k_{*0}+\Delta k_*$ after the time point t_0. The presented values stem from the 'best' models chosen in Table 1. Parameter values for model M_0 and model M_0^* are given for comparison.

RHPS4	(0 nM)	0 nM	50 nM	100 nM	1 μM
Model	M_0	M_0^*	M_1^{**}	M_1^*	M_1^*
T_X	10.6	10.6	13.2	7.18	12.4
T_Y	3.21	3.22	3.16	4.07	4.70
T_Z	5.02	5.01	2.08	7.37	8.23
T_d	19.8	19.8	20.8	20.1	27.3
k_{XY}	2.03	2.03	1.82	2.98	1.72
k_{YZ}	7.47	7.45	7.59	5.90	5.10
k_{ZX}	4.78	4.79	9.84	3.26	2.92
t_0	–	–	5.12	2.46	1.68
$k_{X\bar{X}0}$	2.36×10^{-1}	2.35×10^{-1}	–	3.61×10^{-1}	2.11×10^{-1}
$k_{Y\bar{Y}0}$	4.87×10^{-17}	–	–	–	–
$k_{Z\bar{Z}0}$	3.28×10^{-16}	–	1.72	–	–
$k_{X\bar{X}0}+\Delta k_{X\bar{X}}$	2.36×10^{-1}	2.35×10^{-1}	3.21	3.13	1.86
$k_{Y\bar{Y}0}+\Delta k_{Y\bar{Y}}$	–	–	2.90	1.58	8.88×10^{-1}
$k_{Z\bar{Z}0}+\Delta k_{Z\bar{Z}}$	–	–	5.98	1.44	1.36
k_{XA}	1.63×10^{-1}	1.70×10^{-1}	–	7.05×10^{-2}	2.56×10^{-2}
k_{YA}	1.20×10^{-14}	–	–	–	–
k_{ZA}	4.54×10^{-1}	–	1.71×10^{-1}	–	–

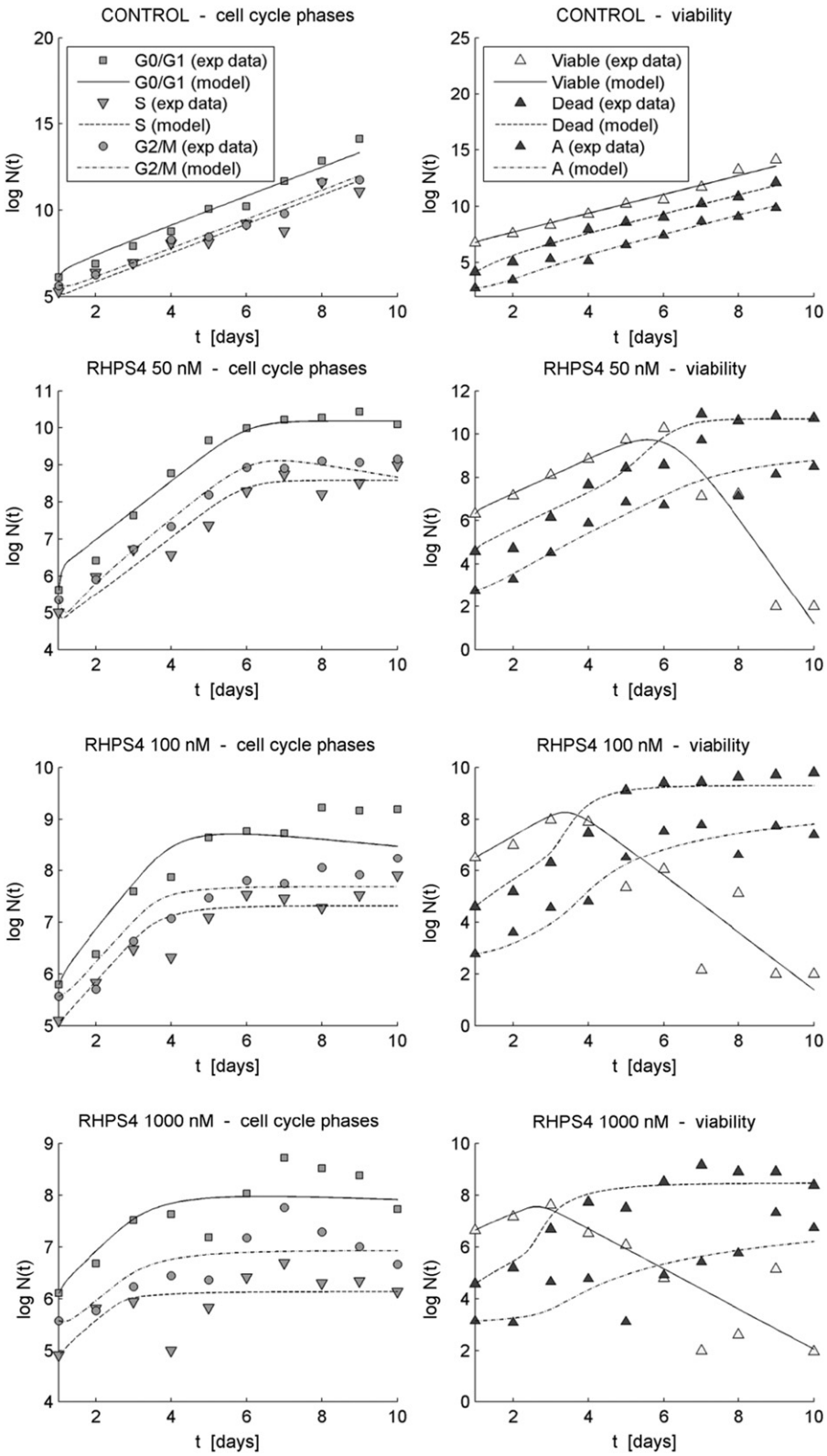

Fig. 8. Solutions of the model fitting procedure to experimental data. Simulations stem from the 'best' models chosen in Table 1. Model curves are represented by lines and experimental data by different markers dependent on the states observed and logarithmic scales have been taken on the vertical axes. 'A' denotes pre-G1 cells and is a subset of nonviable cells. Standard deviations of the experimental data are not shown for better visibility of the markers and would be largely smaller than the symbols.

100 nM, $\xi_s = -0.68232/\text{day}$ for 1 μM RHPS4, setting $k_*(t) = k_{*0} + \Delta k_*$ in Appendix B) which decline markedly with increasing drug concentration. Model analysis revealed that we find oscillations for values of t close to 0, which vanish rapidly as t increases. The peak of the number of viable cells is shifted towards earlier times at increasing drug concentration. The number of pre-G_1 cells grows exponentially for control cells and in the second half of the observation period, linearly for treated cells due to the number of

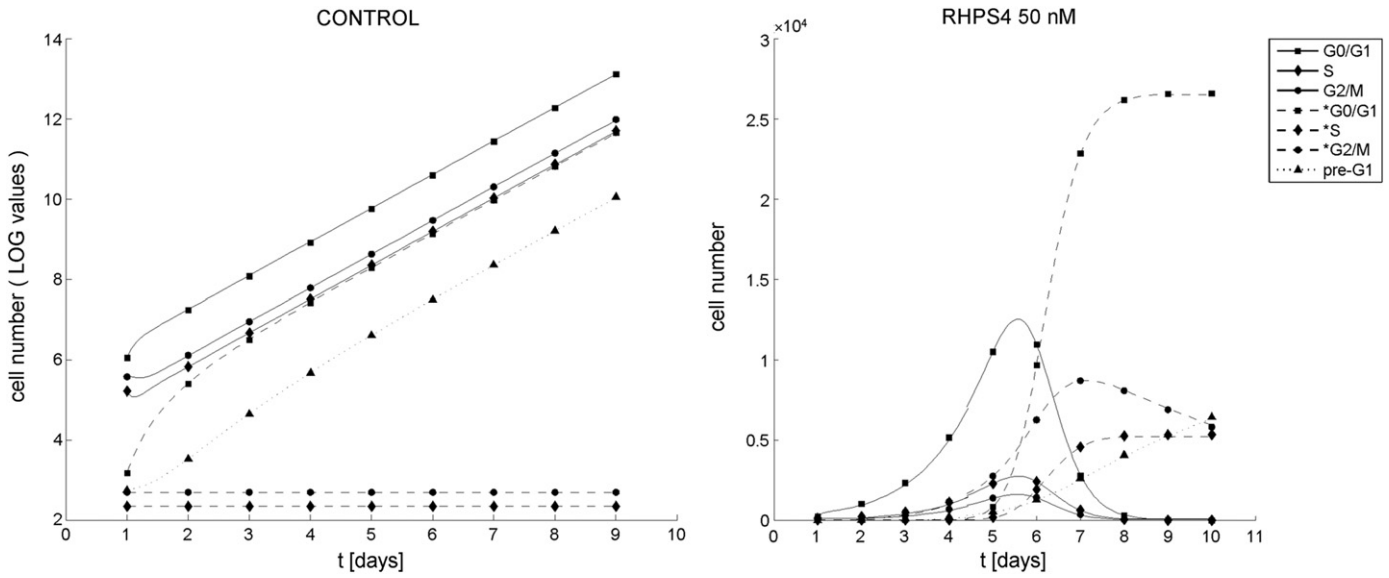

Fig. 9. Cell cycle dynamics simulated for the behaviour of control cells (left: log-plot for better visual distinction between the different phases of the cell cycle) and for the behaviour of cells treated with 50 nM of RHPS4 (right: normal scale on vertical axis). The asterisk in front of phase names in the legend denotes dead cells.

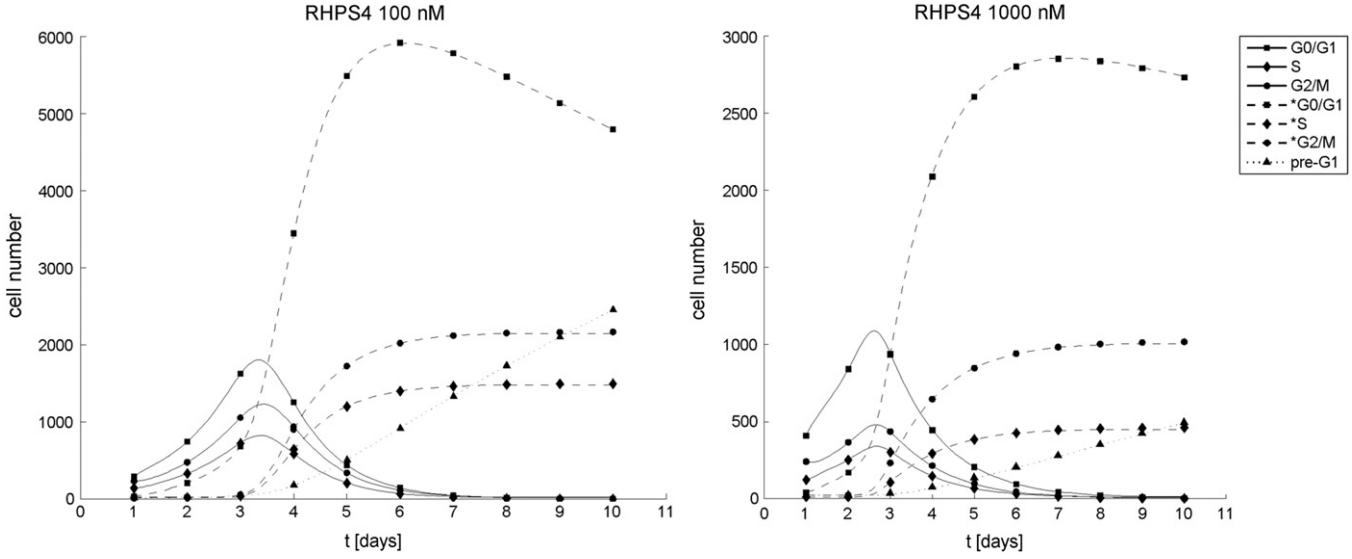

Fig. 10. Cell cycle dynamics simulated for the behaviour of cells treated with 100 nM (1 μM) of RHPS4 are shown on the left (right) side of this figure. Simulations stem from model fitting to experimental data. The asterisk in front of phase names in the legend denotes dead cells.

dead cells ceasing to proliferate. For the lowest drug concentration of 50 nM, however, the model predicts a higher number of viable S-phase cells than viable G_2/M-phase cells across the observation period contrary to respective trends for control cells, 100 nM and 1 μM treatments.

Table 2 displays all estimated rate parameter values and some derivations such as doubling times for each concentration of RHPS4. Control cells spend about 10.6 h in the G_0/G_1 phase, 3.2 h in the S phase and 5.0 h in the G_2/M phase according to the fitted parameters. The rates of transition between compartments of viable cells and the average amounts of time T_X, T_Y, T_Z (see Appendix B for definition) a cell spends in each of the cell cycle phases X, Y, Z, do not display a trend with respect to changes in drug concentration. Notable changes predicted by the models, however, are in T_Z for 50 nM, being less than half the length of the corresponding estimates for control cells, and in T_Z for 100 nM and 1 μM, being about 1.5 times this length. The time point t_0 around which the transition rates to cell death increase by Δk_*, with $k_*(t_0) = k_{*0} + \Delta k_*/2$, decreases from 5.12 days to 1.68 days with increasing drug concentration, where the decrease is more significant for the lower drug concentrations than for 1 μM RHPS4.

There is no visible trend predicted by the model for cells dying before the time point t_0. Control cells and cells treated with higher drug concentrations die with lower rates ($k_{X\overline{X}0} < 0.4$/day) from the G_0/G_1 phase, cells treated with 50 nM die markedly ($k_{Z\overline{Z}0} = 1.72$/day) from the G_2/M phase. There is practically no death from the S phase before t_0. After the time point t_0, treated cells die with significantly higher rates from *all* phases of the cell cycle. In particular, cells treated with 50 nM RHPS4 undergo cell death from G_2/M with a markedly higher rate ($k_{Z\overline{Z}0} + \Delta k_{Z\overline{Z}} = 5.98$/day) than from the other cell cycle phases. DNA degradation in cells occurs largely from each of the phases of the cell cycle in which cells die before the time point t_0.

4.4. Accuracy of fit

We evaluate how accurate our chosen model reflects the properties of the collected data by employing statistical significance tests. In writing down model (12), we have made several assumptions, namely that the model describes the underlying dynamics sufficiently accurately, and that errors are independent and log-normally distributed with the same standard deviation σ. Under the model the residuals $\mathbf{e}_{i,j}$ are independent with a $N(0,\sigma^2)$ distribution. Using the Anderson–Darling Statistic (Stephens, 1974, 1976) we found no evidence at a 5% significance level against the hypothesis that $\mathbf{e}_{i,j} \sim N(0,\sigma^2)$. Furthermore, using a t-statistic (Kraemer, 1975) we found no evidence against the assumption that residuals are independent. We also have not found any significant autocorrelation (Cedersund and Roll, 2009), that is $\mathbf{e}_{i+1,j}$ being correlated with $\mathbf{e}_{i,j}$, $i=1,\ldots,n-1$, over the time points of observation in the residuals. Most of the p-values were larger than 0.5, none of them being smaller than 0.15. The level of correlation in residuals for control and at 50 nM RHPS4 is very low ($p>0.1$ for most pairs of residuals), indicating that our models capture the dynamics well. Fig. 11 displays the residuals $\mathbf{e}_{i,j}$ for the case of 50 nM of RHPS4. For higher drug concentrations, we find statistically significant ($p<0.05$) correlation between residuals from $X+\overline{X}$, $Y+\overline{Y}$, $Z+\overline{Z}$, $\overline{X}+\overline{Y}+\overline{Z}+A$, indicating that there is some systematic variability in the data that the model does not capture. The near-linear relationships between residuals may be caused by secondary dynamics in nonviable cells, which are not accounted for in our model.

An illustration of the estimates of the rate parameters for the four RHPS4 assays with respective standard errors is given in Fig. 12. Standard errors correspond to local analysis around $\hat{\mathbf{p}}$ and, therefore, large error bars indicate low accuracy in a neighbourhood around the optimal parameter. Consequently, error bars do not indicate the full range of possible parameter values for the model to be a good prediction of the cell cycle dynamics.

The degree of correlation in the model parameters was evaluated by computing the correlation matrix of $\hat{\mathbf{p}}$ (see Appendix C) for each drug concentration. For the control case and higher drug concentrations, we found only weak correlation between parameters. There is, however, a positive correlation between k_{ZX} and $k_{Z\overline{Z}0}$ for treated cells with 50 nM RHPS4, meaning that, with parameter values being at the current level, certain proportional changes in k_{ZX} and $k_{Z\overline{Z}0}$ do not significantly influence the model predictions in a close neighbourhood of the estimated parameter values. Hence, good predictions for these parameters lie within a narrow ellipsoidal region in the k_{ZX}–$k_{Z\overline{Z}0}$-plane, whose orientation and length of principal axes can be estimated (Draper and Smith, 1998). Thus, the parameter values can be slightly lower or higher but must approximately satisfy $k_{ZX} \approx 5\, k_{Z\overline{Z}0}$. Lower accuracy and strong correlation between k_{ZX} and $k_{Z\overline{Z}0}$ suggest that the drug effects on these parameters may be less dramatic at 50 nM RHPS4 than originally inferred from model fitting.

4.5. Biological implications

We find that the drug affects the cell cycle phases differently at lower and higher concentrations. High concentrations do not have a cell-cycle specific effect on cells over the total observation period, whereas low concentrations seem to affect the G_2/M phase by increasing the rate of transition to the G_0/G_1 phase indicating fewer or faster processes occurring in the G_2/M phase, which simultaneously introduce marked cell death from G_2/M over the period of observation.

Furthermore, we observe a drug-dependent behaviour in terms of cells undergoing cell death around t_0 (the time point of significant cell death), where higher drug doses reduce the delay to the onset of marked cell death, which occurs in a largely cell-cycle independent manner. The delay in the effects of the drug can be interpreted either as the time which the drug requires

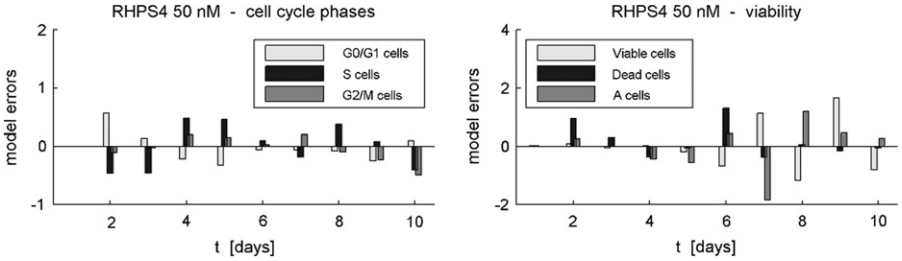

Fig. 11. Residuals $\mathbf{e}_{i,j}$ for time points t_i, $i=1,\ldots,10$, and model categories $j=1,\ldots,6$, are plotted on the time scale for model M_1^{**} and experimental data from treatment with 50 nM of RHPS4, respectively. There is no evidence at a 5% level (Anderson–Darling Statistic) against the null hypothesis that the residuals are sampled from a normal distribution. 'A cells' in the legend denotes pre-G1 cells.

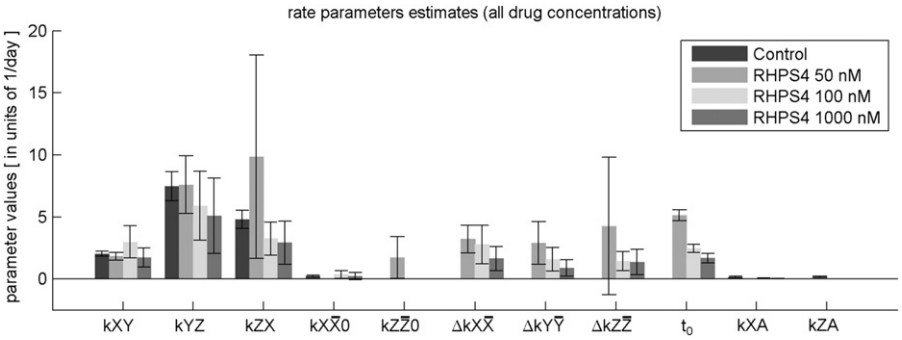

Fig. 12. Parameter estimates for control cells and treatment of cells with 50 nM, 100 nM and 1000 nM RHPS4 from fitting model M_0^* (control), model M_1^* and model M_1^{**} (treated cells). Standard errors of parameter estimates result from model fit to experimental data and are shown by error bars.

to enforce its mechanism of action until the cell's repair machinery is depleted, or as the number of cell divisions required before the drug causes the occurrence of secondary effects leading to cell death.

5. Discussion and conclusions

We have shown that the perception of how the drug RHPS4 affects the cell cycle dynamics is oversimplified. This was achieved by choosing a method of analysis which provides more information on cell cycle dynamics, and more information on the accuracy of obtained results.

We have combined two different approaches in this work: we conducted our own experiments and used our measurements for model fitting. Colorectal cancer cells were plated in media with different concentrations of RHPS4 for up to 10 days and their growth properties and cell cycle distribution analysed. The dip in the total numbers of control cells at day 10 is likely to result from environment-dependent growth inhibition, as the media has not been replaced throughout the experiments in order not to interfere with the cells' natural environment. Also, the number of cells at day 1 was slightly lower than the value of the initial number of cells at seeding (day 0), indicating that cells did not replicate during the first day after seeding. This can also be partly due to not all cells attaching to the bottom of the well after seeding in media. For simplicity of analysis, we considered day 1 as the start ($t=0$) of the analysis of cell cycle modelling.

As well as cell cycle analysis, we measured the proportion of nonviable cells by trypan blue dye-exclusion, as DNA degradation is not an early event of apoptosis and, therefore, should not be taken as the indicator of cell death (Vermes et al., 2000). Apoptotic cells and other dead cells split into apoptotic bodies and their DNA degradation takes place after the onset of cell death. Inaccuracies in measuring the fractions of pre-G_1 cells can arise from one or more of the following: firstly, on death, one cell can produce several fragments each with some DNA content. Secondly, cells can undergo apoptosis from all phases of the cell cycle, hence debris from a single S or G_2/M cell may not be detected as 'pre-G_1' at all (Kajstura et al., 2007) as it has the DNA content of a normal cell (in G_0/G_1). Since these reasons include arguments for under- and overestimation of the actual proportion of late-apoptotic cells, our method of deriving the pre-G_1 fraction can be taken as a good indication for the frequency of apoptotic cells.

The experimental data were used to fit models of cell cycle dynamics and the best fit has been identified. However, model residuals show some correlations between state variables for higher concentrations of RHPS4. There was a decisive reduction in the number of cells treated with 1 μM RHPS4 between days 7 and 10. In particular, the number of harvested cells incubated for more than 7 days decreased although the respective seeding densities were the same in these experiments. Dead cells split into apoptotic bodies and disintegrate in the media making it hard to detect such cells when counted. Indeed, cell debris was observed while cells were counted, and a complete disintegration of apoptotic bodies in the media may have been a reason for underestimating the number of dead cells as well as the number of pre-G_1 cells towards the end of the observation period.

We report that cells from the HCT116 cell line are affected by the drug in the S phase after 4 days when the fraction of cells in this phase drops by 10–20%. The rather temporary effect indicates that in many treated cells, the effect of the drug is to prevent cells passing the G_1–S check point where a cell commits to the synthesis phase of cell division. This can be due to cells resolving certain chromosome replication defects introduced by the drug until cellular conditions are favourable for the cell division cycle. The decrease in S (and consequently G_2/M) phase cells, however, is only one minor effect of the treatment and we could not fully explain its causes by our model.

More significant is the delayed onset of rapid cell death within the population of treated cells, occurring largely from the G_2/M phase for 50 nM and from the G_0/G_1 phase for higher concentrations of RHPS4. The delay decreases with higher drug concentrations and the mechanisms for the delay remain to be discovered. RHPS4 stabilises G-quadruplexes, which has been found to inhibit telomerase (Gowan et al., 2001), it thus shortens telomeres during replication. This could cause increased senescence of treated cells. The drug also causes telomere uncapping leading to apoptosis (Salvati et al., 2007). We suggest that RHPS4 affects telomeres of colorectal cancer cells in two ways: first, induced telomere shortening may decrease the fraction of telomeres being in a capped state (Rodriguez-Brenes and Peskin, 2010), and additional disruption of telomeric proteins may subsequently cause damage to the uncapped telomeres leading to activation of damage response pathways in cells traversing S phase (Rizzo et al., 2009). These findings could serve as a potential explanation in particular for the late death of cells treated with 50 nM RHPS4, which we found occurs largely from the G_2/M phase. Secondly, higher concentrations of the drug may lock the telomeric end in G-quadruplex structures causing severe replication stress by impairing fork progression in early S phase, which could explain the earlier onset of cell death for 100 nM and 1 μM of the drug. G-quadruplexes seem not to be compatible with chromosome replication: they have been observed *in vivo* throughout the cell cycle except for the phase of DNA replication (Lipps and Rhodes, 2009).

In summary, we have shown that the compound RHPS4 has a concentration-dependent effect on the proliferation of HCT116 cells and affects cell cycle progression at an early stage of incubation with the drug. Similar to interpretations of RHPS4-related effects in Rizzo et al. (2009), who exposed HCT116 cells to the drug for 10 days, collected data at day 4, 6, 8, 10, and found significant growth inhibition, we suggest that RHPS4 interferes with the replication fork during DNA synthesis, causing DNA damage and apoptosis. Cells may initially recover rapidly from the replication stress, explaining the dip in the S phase proportions at day 4 with a slight, subsequent increase, but eventually undergo cell death due to the inability to fix further defects. One explanation is that RHPS4 stabilises G4 structures at the telomeric end creating a barrier for DNA strand replication; mathematical modelling of telomere replication processes with interference through G4 formation will be part of our future investigations.

Supplementary material

SRES is a stochastic optimisation algorithm and, therefore, several runs have to be evaluated to determine the global minimum, see the figure in the Supplementary material: optimal parameter values from the global (SRES, grey dots) and local optimisation routine (LM, black dots) for 30 runs are plotted with their optimal function value for a choice of eight parameters, each run being represented by a dotted line connecting the initial guess (optimal value from SRES) and the optimal value from the LM routine. The parameter set that resulted in the overall lowest cost function value has been chosen and is circled in this figure. Results of fitting model M_1^{**} to experimental data from treatment with 50 nM of RHPS4 are shown with the parameter values being given in units of 1/day. The optimal parameters of the 30 fits do not differ more than 0.5/day from the parameter value with the lowest cost function value for each of the different parameters, only the convergence of k_{ZX} and $\Delta k_{Z\overline{Z}}$ is less stable with a spectrum of about ± 2.5/day and ± 2/day, respectively.

Acknowledgments

We thank all members of the Pharmacology Group at the Centre for Biomolecular Science, University of Nottingham, for their introduction, comments and support with the experiments in the tissue culture lab. We also thank the School of Mathematical Sciences, University of Nottingham, for funding this work.

Appendix A. Experimental procedures

A.1. Suppliers of reagents

We purchased reagents from the following suppliers: FlowCheck® beads: Beckman Coulter Ltd., Buckinghamshire, UK; Industrial methylated spirits (IMS): Fisher Scientific Ltd., Leicestershire, UK; 3,11-difluoro-6,8,13-trimethyl-8*H*-quino[4,3,2-kl] acridinium methosulfate (RHPS4): Pharminox Ltd., Nottingham, UK; Dimethylsulphoxide (DMSO), foetal bovine serum (FBS), Ribonuclease A from bovine pancreas (RNAse A), RPMI 1640 liquid medium (containing 0.3 g/L L-glutamine and 2 g/L sodium bicarbonate), phosphate buffered saline (PBS) tablets, propidium iodide (PI) (HPLC grade), sodium citrate, Titron X-100, trypsin-EDTA 1 × solution, Trypan blue: Sigma-Aldrich Co. Ltd., Dorset, UK.

A.2. Drug stock and general cell culture

We used the HCT116 cell line for the biological experiments, which is one of three strains of human malignant cells isolated from a male with colonic carcinoma. HCT116 cells grow in a monolayer and have a relatively short doubling time of 20.5 h (Brattain et al., 1981). The cell line has been chosen because of its good sensitivity to RHPS4 and reliable growth properties which allow analysis of cell viability and cell cycle analysis.

RHPS4 is a water-soluble compound, which facilitates rapid uptake into cells, and it appeared to be localised in the nuclear membrane, intranuclear bodies and cytoplasm (Cookson et al., 2005b). HCT116 colorectal cancer cells were incubated in the pentacyclic acridinium salt RHPS4 at different concentrations to analyse its action on the cells for periods of up to 10 days. The stock of RHPS4 was prepared at a concentration of $c_{st} = 10$ mM in DSMO and stored at 4 °C protected from light. The desired concentrations c_{as} used in assays of $V_{as} = 2$ ml each were obtained by adding a volume of $V_{st} = c_{as}V_{as}/(c_{st} - c_{as})$ from the drug stock. As V_{st} is of a smaller order than 10^{-3} ml for the concentrations of 50 nM, 100 nM and 1 μM used in the assays, the change of volume in the assays is negligible.

All cell culture techniques were carried out aseptically in a BioMat^2 MDH Class II microbiological safety cabinet with a laminar flow system. Cells were maintained in Costar tissue flasks (25 cm^2 and 75 cm^2) with RPMI 1640 medium, containing additionally 10% heat-inactivated FBS. FBS was heat inactivated by heating to 55−59°C for 1 h, and cooled before addition to RPMI tissue culture media.

To seed cells at a certain density, all RPMI tissue culture was aspirated from the flasks and briefly rinsed with sterile PBS. Cells were detached from the flask with 1 ml trypsin-EDTA per 25 cm^2 and resuspended in 6 ml RPMI tissue culture media. The cells were syringed through a 23 G needle to obtain a near-single suspension. The total number of cells in the flask was derived by taking two samples from the flask to count the number of cells within each sample using a haemocytometer and taking the average. The cells were seeded at the desired density of cells by suspending the appropriate amount of cells in RPMI tissue culture media.

HCT116 cells were then grown in 6-well plates in a total volume of 2 ml of RPMI tissue culture medium per 9.6 cm^2 well and maintained at 37 °C in a 5% CO^2, humidified atmosphere until preparation for analysis. The initial cell densities vary between 1000 and 200,000 cells per well dependent on the length of time of incubation, in order to guarantee a confluence level, that is, the fraction of surface area in the well covered by cells, of less than 80% on the day of analysis (to maximise the proportion of cycling cells). Cells were incubated for about 5 h or until attached to the bottom of each well. Treatment of cells with 50 nM, 100 nM or 1 μM of RHPS4 was carried out and cells were reincubated in unmodified conditions. Cells were not passaged before the day of analysis, and they grew at different rates according to drug concentration and duration for which they were incubated.

A.3. Cell cycle analysis

The protocol used for the cell cycle analysis of the HCT116 cell line was adapted from Riccardi and Nicoletti (2006). To harvest the cells, all RPMI tissue culture media, possibly containing dead cells and debris, were collected in FACS tubes and the remaining cells detached from the flask with 350 μl trypsin-EDTA per well. The cells were resuspended in the collected tissue culture media and transferred back into FACS tubes. About 1 ml of PBS solution was used to wash off the empty wells and to transfer the resulting solution to the FACS tubes to ensure an as accurate cell count as possible. To pellet the cells, they were centrifuged at 1200 rpm for 5 min at 4 °C and the supernatant removed. The cell pellet was, depending on the number of cells, resuspended in 100–500 ml of PBS and the suspension syringed through a 23 G needle. About 15 μl of the suspension was mixed with 15 μl of 0.4% trypan blue (staining non-viable cells blue) in microcentrifuge tubes and the number of viable and dead cells counted in a haemocytometer. The remaining cells were again centrifuged at 1200 rpm for 5 min at 4 °C, the supernatant decanted and the pellet resuspended in 400 μl hypotonic fluorochrome solution, which had been composed of 50 μg/ml propidium iodide, 0.1% sodium citrate, 0.1% Titron X-100 and 0.1 mg/ml RNAse A in distilled water.

The cells were kept at 4 °C for 24 h in the dark prior to analysis in which the PI fluorescence of individual nuclei was measured using a Coulter Epics XL-MCL™ flow cytometer operated using Expo32™ software. Before using the Coulter Epics XL-MCL™ flow cytometer, a quality control check was carried out according to the manufacturer's instructions to monitor instrument alignment using FlowCheck ® beads. When the quality control check was satisfactory, the cells were analysed. List mode data for fluorescence emission in the FL3 channel (representing PI fluorescence) of particles were collected. The flow rate was set to low and a minimum of 20,000 cells was analysed. We used a dot plot of FL3 against AUX (channel for peak fluorescence signal) of all detected events to distinguish single cells from unwanted doublets as described in Nunez (2001).

The proportion of cells in each phase of the cell cycle (pre-G_1, G_1/G_0, S and G_2/M) was estimated by setting gates manually on the DNA content histograms obtained from FL3 fluorescence of single cells and using the software package WinMDI (freeware designed by J. Trotter, allowing the removal of doublets via gating of list mode data).

We are interested in the response of cells to four different levels of the drug and accordingly investigated the cell cycle distribution and cell viability in each assay throughout a period of 10 days. Every experiment was set up with six replicates to assess the variability associated with the cell growth cycle: the cells were incubated and treated with RHPS4, and cell counting was conducted.

The cells were seeded at different seeding densities in 6-well plates, where the seeding densities were chosen carefully as too dense cell-to-cell contacts can inhibit cell growth, but on the other hand, sufficient cell numbers are needed both for meaningful cell cycle analysis and to allow for comparable cell environments across experiments. The seeding densities correspond to estimates of the population growth in each experiment. Higher initial seeding densities were used for treated cells to compensate for reduced population doublings. Contrary to common procedures, we did not split cells during culture, but adjusted seeding densities for each assay in order to minimise disruption of the natural cell growth.

The total number of doublings (TND), for each concentration of the drug, and for each day i of analysis, was computed for each experiment using the formula

$$\mathrm{TND}_i(t) = \frac{\ln N_i(t) - \ln N_i(0)}{\ln 2}, \tag{A.1}$$

where $\mathrm{TND}_i(t)$ and $N_i(t)$ are, at time point t, the total number of doublings and the total number of cells, respectively, from the experiment used to analyse cells at day i. We now assume that the total number of doublings is independent of the initial seeding density and write $\mathrm{TND}_i = \mathrm{TND}$ for all i.

Now we consider an experiment, where all initial seeding densities are identical, and normalise our data by setting $N_i(0) = 10^3$ for all i. The normalised data set can be derived from the original data by

$$N(t) = 10^3 \cdot 2^{\mathrm{TND}(t)} = 10^3 \frac{N_i(t)}{N_i(0)}, \tag{A.2}$$

where $N(t)$ is the total number of cells that have grown from 10^3 cells in t days. The number of cells in each phase of the cell cycle, including the number of viable and dead cells, can then be obtained by multiplying the respective proportions with $N(t)$.

Appendix B. Doubling times/residence times

A quantity of biological interest is the doubling time of cells, which is the period of time required for a population of cells to double its cell numbers. It is a characteristic unit for the description of cell growth providing a more intuitive notion of the long-term impact of growth.

For constant transition rates k, we can approximate the doubling time from the model dynamics by considering the subsystem of Eqs. (1)–(3) in Section 2.1, which represents the cell cycle dynamics of viable cells as illustrated in Fig. 1. The eigenvalues ξ_j of the respective coefficient matrix

$$\mathbf{M} = \begin{pmatrix} -k_{XY} - k_{X\overline{X}} & 0 & 2k_{ZX} \\ k_{XY} & -k_{YZ} - k_{Y\overline{Y}} & 0 \\ 0 & k_{YZ} & -k_{ZX} - k_{Z\overline{Z}} \end{pmatrix}, \tag{B.1}$$

determine the behaviour of X, Y and Z, and if the largest eigenvalue, say ξ_s, is positive, we expect exponential growth behaviour for the total number of cycling cells. The doubling time can in this case be approximated by

$$T_d = \frac{\ln 2}{\xi_s}, \tag{B.2}$$

through solving $2(X(t)+Y(t)+Z(t)) = X(t+T_d)+Y(t+T_d)+Z(t+T_d)$ for large values of t. For exponential decay ($\xi_s < 0$), the absolute value of T_d gives the half-life of the cell population.

The residence time of cells in a particular cell-cycle phase is the average amount of time a cell spends in that phase. For a compartment, say X, with losses from the X compartment only of rate k_{XY}, it is well-known that the probabilistic waiting time, τ_X, to the next transition from X to Y is exponentially distributed with mean $1/k_{XY}$, that is $\tau_X \sim \exp(1/k_{XY})$. We introduce the probabilistically-motivated notion of the residence time, being the expected value of the waiting time, into our deterministic model, and set

$$T_X = \frac{1}{k_{XY}}, \quad T_Y = \frac{1}{k_{YZ}}, \quad T_Z = \frac{1}{k_{ZX}}, \tag{B.3}$$

for the residence times of cells in the X, Y and Z compartments. For non-negligible losses (rate k_{*0}) from any of the three compartments to cell death, we have to correct our formulas for the residence time, and set $T_X = 1/(k_{XY} + k_{X\overline{X}0})$, $T_X = 1/(k_{YZ} + k_{Y\overline{Y}0})$, $T_Z = 1/(k_{ZX} + k_{Z\overline{Z}0})$.

Appendix C. Correlation coefficients for rate parameters

The correlation matrix

$$\widehat{\mathbf{Corr}}(\hat{\mathbf{p}}) = \left(\frac{\hat{\mathbf{\Sigma}}_{ij}}{\sqrt{\hat{\mathbf{\Sigma}}_{ii}\hat{\mathbf{\Sigma}}_{ij}}} \right), \tag{C.1}$$

where $\hat{\mathbf{\Sigma}} = \hat{\mathbf{\Sigma}}(\hat{\mathbf{p}})$ is as defined in Section 3.2, provides us with information on the degree of linear dependence between parameters. The entries of $\widehat{\mathbf{Corr}}(\hat{\mathbf{p}})$, say $r_{ij}(\hat{\mathbf{p}})$, $i,j = 1,\ldots,L$, have the property $|r_{ij}(\hat{\mathbf{p}})| \le 1$, where we have perfect positive (negative) linear relationship between the parameter estimates $\hat{\mathbf{p}}_i$ and $\hat{\mathbf{p}}_j$ for $r_{ij}(\hat{\mathbf{p}}) = 1$ ($r_{ij}(\hat{\mathbf{p}}) = -1$) and no correlation for $r_{ij}(\hat{\mathbf{p}}) = 0$. Table C.1 presents the correlation coefficients for the estimated parameters in model C**.

Appendix D. Supplementary material

Supplementary data associated with this article can be found in the online version, at doi:10.1016/j.jtbi.2011.10.038

Table C.1
Upper triangular part of the correlation matrix $\widehat{\mathbf{Corr}}(\hat{\mathbf{p}})$ computed as in (C.1) for model M_1^{**} and data from treatment with 50 nM RHPS4.

$\hat{\mathbf{p}}_k$	k_{XY}	k_{YZ}	k_{ZX}	$k_{Z\overline{Z}0}$	$\Delta k_{X\overline{X}}$	$\Delta k_{Y\overline{Y}}$	$\Delta k_{Z\overline{Z}}$	t_0	k_{ZA}
k_{XY}	1	−0.3705	−0.7089	−0.5611	0.6719	−0.3118	−0.7014	−0.0160	0.1211
k_{YZ}		1	−0.1513	−0.1607	−0.3471	0.7008	−0.0754	−0.2058	−0.0167
k_{ZX}			1	0.9617	−0.4064	−0.0605	0.6632	0.1068	−0.4296
$k_{Z\overline{Z}0}$				1	−0.2750	−0.0385	0.5167	0.2015	−0.5210
$\Delta k_{X\overline{X}}$					1	−0.3917	−0.7752	0.3833	0.0714
$\Delta k_{Y\overline{Y}}$						1	−0.0711	0.0366	−0.0365
$\Delta k_{Z\overline{Z}}$							1	−0.0261	−0.1145
t_0								1	−0.0351
k_{ZA}									1

References

Aguda, B.D., 2001. Kick-starting the cell cycle: from growth-factor stimulation to initiation of DNA replication. Chaos 11, 269–276.

Akaike, H., 1974. New look at statistical-model identification. IEEE Trans. Autom. Control AC 19, 716–723.

Ashyraliyev, M., Jaeger, J., Blom, J.G., 2008. Parameter estimation and determinability analysis applied to drosophila gap gene circuits. BMC Syst. Biol. 2.

Basse, B., Ubezio, P., 2007. A generalised age- and phase-structured model of human tumour cell populations both unperturbed and exposed to a range of cancer therapies. Bull. Math. Biol. 69, 1673–1690.

Basse, B., Baguley, B.C., Marshall, E.S., Wake, G.C., Wall, D.J.N., 2005. Modelling the flow cytometric data obtained from unperturbed human tumour cell lines: parameter fitting and comparison. Bull. Math. Biol. 67, 1153.

Bedrick, E.J., Tsai, C.L., 1994. Model selection for multivariate regression in small samples. Biometrics 50, 226–231.

Brattain, M.G., Fine, W.D., Khaled, F.M., Thompson, J., Brattain, D.E., 1981. Heterogeneity of malignant-cells from a human colonic-carcinoma. Cancer Res. 41, 1751–1756.

Cedersund, G., Roll, J., 2009. Systems biology: model based evaluation and comparison of potential explanations for given biological data. FEBS J. 276, 903–922.

Cheng, M.K., Modi, C., Cookson, J.C., Hutchinson, I., Heald, R.A., McCarroll, A.J., Missailidis, S., Tanious, F., Wilson, W.D., Mergny, J.L., Laughton, C.A., Stevens, M.F.G., 2008. Antitumor polycyclic acridines. 20. Search for DNA quadruplex binding selectivity in a series of 8,13-dimethylquino 4,3,2-kl acridinium salts: telomere-targeted agents. J. Med. Chem. 51, 963–975.

Cobelli, C., Distefano, J.J., 1980. Parameter and structural identifiability concepts and ambiguities—a critical-review and analysis. Am. J. Physiol. 239, R7–R24.

Cookson, J.C., Dai, F.P., Smith, V., Heald, R.A., Laughton, C.A., Stevens, M.F.G., Burger, A.M., 2005a. Pharmacodynamics of the G-quadruplex-stabilizing telomerase inhibitor 3,11-difluoro-6,8,13-trimethyl-8H-quino 4,3,2-kl acridinium methosulfate (RHPS4) in vitro: activity in human tumor cells correlates with telomere length and can be enhanced, or antagonised, with cytotoxic agents. Mol. Pharmacol. 68, 1551–1558.

Cookson, J.C., Heald, R.A., Stevens, M.F.G., 2005b. Antitumor polycyclic acridines. 17. Synthesis and pharmaceutical profiles of pentacyclic acridinium salts designed to destabilise telomeric integrity. J. Med. Chem. 48, 7198–7207.

Draper, N.R., Smith, H., 1998. Applied Regression Analysis, Wiley Series in Probability and Statistics. Texts and References Section, third ed. Wiley, New York, Chichester.

Fuss, H., Dubitzky, W., Downes, C.S., Kurth, M.J., 2005. Mathematical models of cell cycle regulation. Briefings Bioinf. 6, 163–177.

Gavathiotis, E., Heald, R.A., Stevens, M.F.G., Searle, M.S., 2003. Drug recognition and stabilisation of the parallel-stranded DNA quadruplex d(TTAGGGT)(4) containing the human telomeric repeat. J. Mol. Biol. 334, 25–36.

Gowan, S.M., Heald, R., Stevens, M.F.G., Kelland, L.R., 2001. Potent inhibition of telomerase by small-molecule pentacyclic acridines capable of interacting with G-quadruplexes. Mol. Pharmacol. 60, 981–988.

Jacquez, J.A., 1996. Compartmental analysis in biology and medicine, third ed. BioMedware, Ann Arbor, MI.

Johnson, L.A., Byrne, H.M., Willis, A.E., Laughton, C.A., 2011. An integrative biological approach to the analysis of tissue culture data: application to the antitumour agent RHPS4. Integr. Biol. 3, 843–849.

Kajstura, M., Halicka, H.D., Pryjma, J., Darzynkiewicz, Z., 2007. Discontinuous fragmentation of nuclear DNA during apoptosis revealed by discrete "sub-G(1)" peaks on DNA content histograms. Cytomet. Part A 71A, 125–131.

Kim, N.W., Piatyszek, M.A., Prowse, K.R., Harley, C.B., West, M.D., Ho, P.L.C., Coviello, G.M., Wright, W.E., Weinrich, S.L., Shay, J.W., 1994. Specific association of human telomerase activity with immortal cells and cancer. Science 266, 2011–2015.

Kleinstein, S.H., Bottino, D., Lett, G.S., Georgieva, A., Sarangapani, R., 2006. Nonuniform sampling for global optimization of kinetic rate constants in biological pathways. Proceedings of the 2006 Winter Simulation Conference, vol. 1–5; 2006, pp. 1611–1616.

Koch, A.L., 1966. Logarithm in biology. 1. Mechanisms generating log-normal distribution exactly. J. Theoret. Biol. 12, 276–290.

Kraemer, H.C., 1975. Estimation and hypothesis testing problems for correlation-coefficients. Psychometrika 40, 473–485.

Leonetti, C., Amodei, S., D'Angelo, C., Rizzo, A., Benassi, B., Antonelli, A., Elli, R., Stevens, M.F.G., D'Incalci, M., Zupi, G., Biroccio, A., 2004. Biological activity of the G-quadruplex ligand RHPS4 (3,11-difluoro-6,8,13-trimethyl-8*H*-quino 4,3,2-kl acridinium methosulfate) is associated with telomere capping alteration. Mol. Pharmacol. 66, 1138–1146.

Levy, M.Z., Allsopp, R.C., Futcher, A.B., Greider, C.W., Harley, C.B., 1992. Telomere end-replication problem and cell aging. J. Mol. Biol. 225, 951–960.

Limpert, E., Stahel, W.A., Abbt, M., 2001. Log-normal distributions across the sciences: keys and clues. Bioscience 51, 341–352.

Lipps, H.J., Rhodes, D., 2009. G-quadruplex structures: in vivo evidence and function. Trends Cell Biol. 19, 414–422.

Montalenti, F., Sena, G., Cappella, P., Ubezio, P., 1998. Simulating cancer-cell kinetics after drug treatment: application to cisplatin on ovarian carcinoma. Phys. Rev. E 57, 5877–5887.

Nunez, R., 2001. DNA measurement and cell cycle analysis by flow cytometry. Curr. Issues Mol. Biol. 3, 67–70.

Panetta, J.C., Adam, J., 1995. A mathematical-model of cycle-specific chemotherapy. Math. Comput. Model. 22, 67–82.

Riccardi, C., Nicoletti, I., 2006. Analysis of apoptosis by propidium iodide staining and flow cytometry. Nat. Protoc. 1, 1458–1461.

Rizzo, A., Salvati, E., Porru, M., D'Angelo, C., Stevens, M.F., D'Incalci, M., Leonetti, C., Gilson, E., Zupi, G., Biroccio, A., 2009. Stabilization of quadruplex DNA perturbs telomere replication leading to the activation of an ATR-dependent ATM signaling pathway. Nucl. Acids Res. 37, 5353–5364.

Rodriguez-Brenes, I.A., Peskin, C.S., 2010. Quantitative theory of telomere length regulation and cellular senescence. Proc. Natl. Acad. Sci. USA 107, 5387–5392.

Runarsson, T.P., Yao, X., 2000. Stochastic ranking for constrained evolutionary optimization. IEEE Trans. Evol. Comput. 4, 284–294.

Salvati, E., Leonetti, C., Rizzo, A., Scarsella, M., Mottolese, M., Galati, R., Sperduti, I., Stevens, M.F.G., D'Incalci, M., Blasco, M., Chiorino, G., Bauwens, S., Horard, B., Gilson, E., Stoppacciaro, A., Zupi, G., Biroccio, A., 2007. Telomere damage induced by the G-quadruplex ligand RHPS4 has an antitumor effect. J. Clin. Invest. 117, 3236–3247.

Seber, G.A.F., Wild, C.J., 1989. Nonlinear Regression. Wiley Series in Probability and Mathematical Statistics. Wiley, New York, Chichester.

Sherer, E., Tocce, E., Hannemann, R.E., Rundell, A.E., Ramkrishnal, D., 2008. Identification of age-structured models: cell cycle phase transitions. Biotechnol. Bioeng. 99, 960–974.

Stephens, M.A., 1974. EDF statistics for goodness of fit and some comparisons. J. Am. Stat. Assoc. 69, 730–737.

Stephens, M.A., 1976. Asymptotic results for goodness-of-fit statistics with unknown parameters. Ann. Stat. 4, 357–369.

Tyson, J.J., 1991. Modeling the cell-division cycle—cdc2 and cyclin interactions. Proc. Natl. Acad. Sci. USA 88, 7328–7332.

Tyson, J.J., Novak, B., 2001. Regulation of the eukaryotic cell cycle: molecular antagonism, hysteresis, and irreversible transitions. J. Theoret. Biol. 210, 249–263.

Venkatasubramanian, R., Henson, M.A., Forbes, N.S., 2008. Integrating cell-cycle progression, drug penetration and energy metabolism to identify improved cancer therapeutic strategies. J. Theoret. Biol. 253, 98–117.

Vermes, I., Haanen, C., Reutelingsperger, C., 2000. Flow cytometry of apoptotic cell death. J. Immunol. Methods 243, 167–190.

Walter, E., Pronzato, L., 1996. On the identifiability and distinguishability of nonlinear parametric models. Math. Comput. Simul. 42, 125–134.

Wolkenhauer, O., Fell, D., De Meyts, P., Bluthgen, N., Herzel, H., Le Novere, N., Hofer, T., Schurrle, K., van Leeuwen, I., 2009. Sysbiomed report: advancing systems biology for medical applications. IET Syst. Biol. 3, 131–136.

Yang, L., Han, Z.G., MacLellan, W.R., Weiss, J.N., Qu, Z.L., 2006. Linking cell division to cell growth in a spatiotemporal model of the cell cycle. J. Theoret. Biol. 241, 120–133.